The gain enhancement effect of surface plasmon polaritons on terahertz stimulated emission in optically pumped monolayer graphene

2013 New J. Phys. 15 075003

(http://iopscience.iop.org/1367-2630/15/7/075003)

New Journal of Physics
The open access journal for physics

The gain enhancement effect of surface plasmon polaritons on terahertz stimulated emission in optically pumped monolayer graphene

Takayuki Watanabe[1,4], Tetsuya Fukushima[1], Yuhei Yabe[1], Stephane Albon Boubanga Tombet[1], Akira Satou[1], Alexander A Dubinov[2], Vladimir Ya Aleshkin[2], Vladimir Mitin[3], Victor Ryzhii[1] and Taiichi Otsuji[1]

[1] Research Institute of Electrical Communication, Tohoku University, Sendai 9808577, Japan
[2] Institute for Physics of Microstructures, Russian Academy of Sciences, Nizhny Novgorod 603950, Russia
[3] Department of Electrical Engineering, University at Buffalo, State University of New York, NY 14260, USA
E-mail: watanabe@riec.tohoku.ac.jp

New Journal of Physics **15** (2013) 075003 (11pp)
Received 5 May 2013
Published 3 July 2013
Online at http://www.njp.org/
doi:10.1088/1367-2630/15/7/075003

Abstract. Nonlinear carrier relaxation/recombination dynamics and the resultant stimulated terahertz (THz) photon emission with excitation of surface plasmon polaritons (SPPs) in photoexcited monolayer graphene has been experimentally studied using an optical pump/THz probe and an optical probe measurement. We observed the spatial distribution of the THz probe pulse intensities under linear polarization of optical pump and THz probe pulses. It was clearly observed that an intense THz probe pulse was detected only at the area where the incoming THz probe pulse takes a transverse magnetic (TM) mode capable of exciting the SPPs. The observed gain factor is in fair agreement with the theoretical calculations. Experimental results support the occurrence of the gain enhancement by the excitation of SPPs on THz stimulated emission in optically pumped monolayer graphene.

[4] Author to whom any correspondence should be addressed.

Contents

1. Introduction

Graphene has attracted increasing attention for terahertz (THz) and optoelectronic device applications due to its exceptional electronic and optical properties [1–5]. The conduction and valence bands of graphene have a symmetrical conical shape around the Brillouin zone edges, which are called K and K' points, and contact each other at 'Dirac points' at the K and K' points. Electrons and holes in graphene have a linear energy dispersion relation with zero bandgap, resulting in peculiar features such as massless relativistic fermions with back-scattering-free ultrafast transport [1–5] as well as the negative dynamic conductivity at THz frequencies under optical or electrical pumping [6–11]. Interband population inversion in graphene can be achieved by its optical pumping [6, 8] or carrier injection [7, 8] along with the ultrafast nonequilibrium carrier energy relaxation processes. At sufficiently strong excitation, the interband stimulated emission of photons can prevail over the intraband (Drude) absorption. In this case, the real part of the dynamic conductivity of graphene, $\mathrm{Re}[\sigma(\omega)]$, becomes negative at some frequencies ω. Owing to the gapless energy spectrum of graphene, $\mathrm{Re}[\sigma(\omega)]$ can be negative in THz range [6–11]. This effect can be exploited in graphene-based THz lasers with optical or injection pumping [8, 12–14].

The carrier dynamics in optically pumped graphene strongly depends on the initial temperature of carriers and the intensity of optical pumping. For sufficiently low carrier concentrations, that is, at low temperatures under weak pumping, photoexcited carriers accumulate effectively near the Dirac point via the cascade emission of optical phonons (OPs). Under these conditions population inversion can be achieved efficiently [6, 7, 9]. In contrast, at room temperature or under stronger pumping, where the carrier concentration is high ($10^{12}\,\mathrm{cm}^{-2}$), carrier–carrier (CC) scattering plays a crucial role in the dynamics after pulse excitation, because of the fast quasi-equilibration of the carriers [15–17]. Ultrafast optical pump–probe spectroscopy on graphene has indicated that the quasi-equilibration by CC scattering occurs on a time scale of 10–100 fs [15–17], which is much faster than a single OP emission. In this case, the pulse excitation makes carriers very hot initially, and the energy relaxation and recombination via OP emission follow [9]. Under these conditions for intrinsic graphene at room temperature, population inversion can still be achievable when the pumping intensity exceeds a certain threshold level [9, 11].

Li *et al* [18] observed stimulated emission of near-infrared photons in femtosecond (fs) infrared (IR) laser-pumped graphene at very short time durations just 10 s of femtoseconds after the pumping, which was before the photoexcited carriers were quasi-equilibrated by the CC scattering. The authors, on the other hand, observed stimulated emission of THz photons [19, 20] from fs-IR laser-pumped monolayer graphene at the time duration a few picoseconds after the pumping when photoexcited carriers were quasi-equilibrated and their populations were inverted at THz photon energies beyond the Dirac point. We utilized a time-resolved near-field reflective electro-optic sampling with a fs-IR laser pulse for optical pumping and a synchronously generated THz pulse for probing the THz dynamics of the sample in a THz photon-echo manner [19]. The gain spectral profiles showed qualitative agreement with theory in terms of threshold behavior against the pumping intensity, normal dispersion around the gain peak frequency and gain spectral narrowing particularly at the higher frequency band edge [6, 11, 13, 19]. However, the obtained gain factor exceeds the theoretical limit given by the quantum conductance [21] by more than one order of magnitude. We consider any artifact caused in experimental setup (gain multiplication due to multiple reflection, reflective index change due to increase in free carriers, etc), [19] but cannot explain such a phenomenon.

One possibility is the amplified stimulated plasmon emission by the excitation of surface plasmon polaritons (SPPs), which was theoretically revealed by the authors [22]. Two-dimensional plasmons in graphene exhibit unique optoelectronic properties and mediate extraordinary light–matter interactions [5] which is expected to be exploited for advanced THz-active devices [5, 22–25]. In this paper, we experimentally study the nonlinear carrier relaxation/recombination dynamics and resultant stimulated THz photon emission with the excitation of SPPs in photoexcited monolayer graphene. We observe the spatial distribution of the THz probe pulse intensities and its dependence on the polarizations of optical pump and THz probe pulses. Intense THz probe pulse is detected only at the area where the incoming THz probe pulse takes a TM mode capable of exciting the SPPs. The observed gain factor is in fair agreement with the theoretical calculations. Experimental results support the occurrence of the gain enhancement effect by the excitation of SPPs on THz stimulated emission in optically pumped monolayer graphene.

2. Stimulated terahertz (THz) photon and plasmon emission in optically pumped graphene

In high-frequency (from THz to infrared) range, the graphene conductivity is derived from the Kubo formula in the following form [21]:

$$\sigma_{\mathbf{k}\omega} = \frac{\mathrm{i}e^2}{\hbar\pi^2}\sum_{a=1,2}\int \frac{\mathrm{d}^2\mathbf{p}v_x^2\{f[\varepsilon_a(\mathbf{p}_-)] - f[\varepsilon_a(\mathbf{p}_+)]\}}{[\varepsilon_a(\mathbf{p}_+) - \varepsilon_a(\mathbf{p}_-)][\hbar\omega - \varepsilon_a(\mathbf{p}_+) + \varepsilon_a(\mathbf{p}_-)]} + \frac{2\mathrm{i}e^2\hbar\omega}{\hbar\pi^2}\int \frac{\mathrm{d}^2\mathbf{p}v_{21}v_{12}\{f[\varepsilon_1(\mathbf{p}_-)] - f[\varepsilon_2(\mathbf{p}_+)]\}}{[\varepsilon_2(\mathbf{p}_+) - \varepsilon_1(\mathbf{p}_-)][(\hbar\omega)^2 - [\varepsilon_2(\mathbf{p}_+) - \varepsilon_1(\mathbf{p}_-)]^2]}, \quad (1)$$

where the indices 1 and 2 refer to conduction and valence bands, respectively, $\varepsilon_1(\mathbf{p}) = |\mathbf{p}|\mathrm{v_F}$ and $\varepsilon_2(\mathbf{p}) = -|\mathbf{p}|\mathrm{v_F}$, $v_\mathrm{F} \simeq 10^6\,\mathrm{m\,s^{-1}}$, $\mathbf{p}_\pm = \mathbf{p} \pm \hbar\mathbf{k}/2$, $f(\varepsilon)$ is the electron distribution function (the equilibrium Fermi function $\mathrm{f}(\varepsilon) = 1/[1 + \mathrm{e}^{(\varepsilon-\varepsilon_\mathrm{F})/T}]$ is assumed), $v_x = v_\mathrm{F}\cos\theta_\mathbf{p}$ and $v_{12} = \mathrm{i}v_\mathrm{F}\sin\theta_\mathbf{p}$ is the matrix elements of the velocity operator. The first term in equation (1) corresponds to the intraband transitions, whereas the second term corresponds to the interband

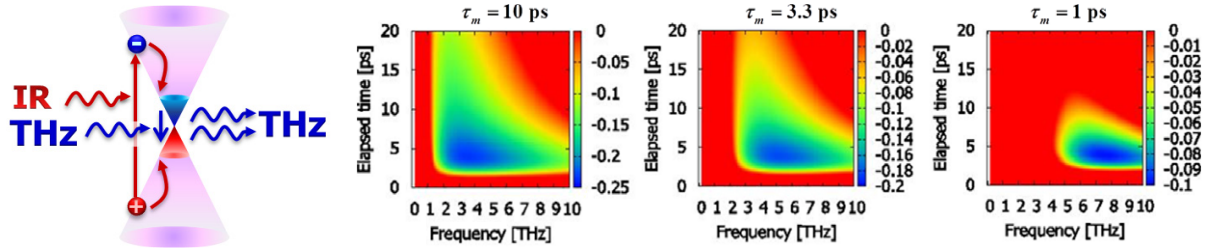

Figure 1. Schematic image of the stimulated THz emission in IR-pumped graphene (left) and numerically simulated temporal evolution of the real part of the dynamic conductivity $\mathrm{Re}[\sigma(\omega)]$ in graphene photoexcited with 0.8 eV, 80 fs pump fluence 8 μJ cm^{-2} (average intensity 1×10^8 cm^{-2}) at the time of 0 ps having different momentum relaxation times τ_m of 10, 3.3 and 1 ps (right). Any positive values of $\mathrm{Re}[\sigma(\omega)]$ are clipped to the zero level (shown in red) to focus on the negative valued region.

transitions. To allow for the electron (hole) momentum relaxation, one should treat the frequency in the intraband part of the conductivity expression as $\omega \to \omega + \mathrm{i}\tau_\mathrm{m}^{-1}$. Then, the real part of equation (1) can be expressed in the following simple form [21]:

$$\mathrm{Re}\,\sigma_\omega = \mathrm{Re}\,\sigma_\omega^{\mathrm{intra}} + \mathrm{Re}\,\sigma_\omega^{\mathrm{inter}} \approx \frac{(\ln 2 + \varepsilon_\mathrm{F}/2k_\mathrm{B}T)e^2}{\pi\hbar} \frac{k_\mathrm{B}T\tau_\mathrm{m}}{\hbar\left(1+\omega^2\tau_\mathrm{m}^2\right)} + \frac{e^2}{4\hbar}(1 - 2f(\hbar\omega)), \tag{2}$$

where e is the elementary charge, $\hbar$ is the reduced Planck's constant, k_B is the Boltzmann constant, T is the temperature and τ_m is the momentum relaxation time of carriers. The intraband contribution, $\mathrm{Re}\,\sigma_\omega^{\mathrm{intra}}$, corresponds to the Drude absorption and is always positive. The THz frequency domain is situated in the intraband Drude conductivity dominated region.

The interband conductivity related to the second term of the right-hand side in equation (2) could take negative values by optical pumping [6, 8] or carrier injection [7, 8], giving rise to the population inversion. At sufficiently strong excitation, the interband stimulated emission of photons can prevail over the intraband (Drude) absorption. In this case, the real part of the dynamic conductivity of graphene, $\mathrm{Re}[\sigma(\omega)]$, becomes negative in THz range [6–11].

Figure 1 shows numerically simulated time evolution of $\mathrm{Re}[\sigma(\omega)]$ for intrinsic graphene at room temperature when graphene is impulsively pumped at the time of zero with photon energy around 0.8 eV [11, 20]. In this simulation quasi-Fermi distribution of carriers due to quasi-equilibration through CC scattering is assumed and Auger-type carrier recombination/multiplication processes [26–28] caused by the crystallographic imperfections or many-body effects under intense photoexcitation are ignored. It is clearly seen that a higher quality of graphene with longer momentum relaxation time and thus less crystallographic defects obtains larger values of negative conductivity in a wider frequency range.

It is worth noting that the negative THz conductivity of monolayer graphene is limited to the quantum conductivity ($e^2/4\hbar$) as seen in equation (3) [21]. This is because the absorption of THz photons that can contribute to the stimulated emission is only made via an interband transition process whose absorbance is limited by $\pi e^2/\hbar c \approx 2.3\%$ [29]. To overcome this limitation on quantum efficiency, a carrier recycling process like that exploited in quantum cascade lasers (QCLs) can be introduced. In this regard, waveguide structures with in-plane THz

photon propagation along the graphene sheet [14] are preferable for comprising the laser cavities in order to maximize the gain overlapping and hence to overcome the quantum mechanical limit in comparison with vertical photon emitting cavity structures [12, 13]. However, even for 20 multiple-layered graphene that can increase the absorbance by almost 20 times, the absorption coefficient of THz photons along the inverted graphene is still relatively low, on the order of $1\,\mathrm{cm}^{-1}$ [14].

As compared with the stimulated emission of the electromagnetic modes (i.e. photons), the stimulated emission of plasmons by the interband transitions in population inverted graphene can be a much stronger emission process. The plasmon gain under population inversion in intrinsic graphene has been theoretically studied in [22]. Nonequilibrium plasmons in graphene can be coupled to the TM modes of electromagnetic waves resulting in the formation and propagation of SPPs [22]. It is shown in [22] that the plasmon gain in pumped graphene can be very high due to small group velocity of the plasmons in graphene and strong confinement of the plasmon field in the vicinity the graphene layer. The propagation constant ρ of the graphene SPP along the z coordinate is derived from Maxwell's equations [22]

$$\sqrt{n^2-\rho^2}+n^2\sqrt{1-\rho^2}+\frac{4\pi}{c}\sigma_\omega\sqrt{1-\rho^2}\sqrt{n^2-\rho^2}=0, \tag{3}$$

where n is the refractive index, c is the speed of light in vacuum and σ_ω is the conductivity of graphene at frequency ω.

The absorption coefficient α is obtained as the imaginary part of the wave vector along the z coordinate: $\alpha = \mathrm{Im}(q_z) = 2\,\mathrm{Im}(\rho\cdot\omega/c)$. Figure 2 plots simulated α for monolayer graphene on a SiO_2/Si substrate ($\mathrm{Im}(n)\sim 3\times 10^{-4}$) at 300 K. To drive graphene in the population inversion with a negative dynamic conductivity, quasi-Fermi energies are parameterized at $\varepsilon_\mathrm{F} = 10$, 20, 30, 40, 50 and 60 meV and a carrier momentum relaxation time $\tau_\mathrm{m} = 3.3$ ps is assumed. The results demonstrate giant THz gain (negative values of absorption) of the order of $10^4\,\mathrm{cm}^{-1}$. Since the absorption coefficients and the resultant gain coefficient (under the negative absorption conditions) directly reflect on the dynamic conductivity σ_ω as shown in equation (3), the gain spectra show similar dependence on momentum relaxation times and thus on the qualities of graphene to that for σ_ω as shown in figure 1.

It is noted that the transverse electric (TE) modes of THz waves can be coupled with graphene plasmons, but basically the propagation along the z coordinate is not allowed so that they do not contribute to any gain enhancement. One possibility is the waveguide TE modes due to the CdTe thin layer (whose refractive index is lower than that of Si even in the THz range), which could propagate along the z coordinate. However, their group velocities are rather higher than those for usual TM SPPs and the overlapping factor for the graphene layer is lower than those for the TM SPPs because the field maximum is located near the middle of the CdTe layer. Therefore, the gain-enhancement effect of these TE modes must be sufficiently lower than those in the TE mode SPPs.

3. Experimental observation of THz stimulated plasmon emission in optically pumped graphene

3.1. Experimental setup and sample preparation

We conducted optical pump, THz probe and optical probe measurement at room temperature for intrinsic monolayer graphene on a SiO_2/Si substrate. The experimental setup is shown

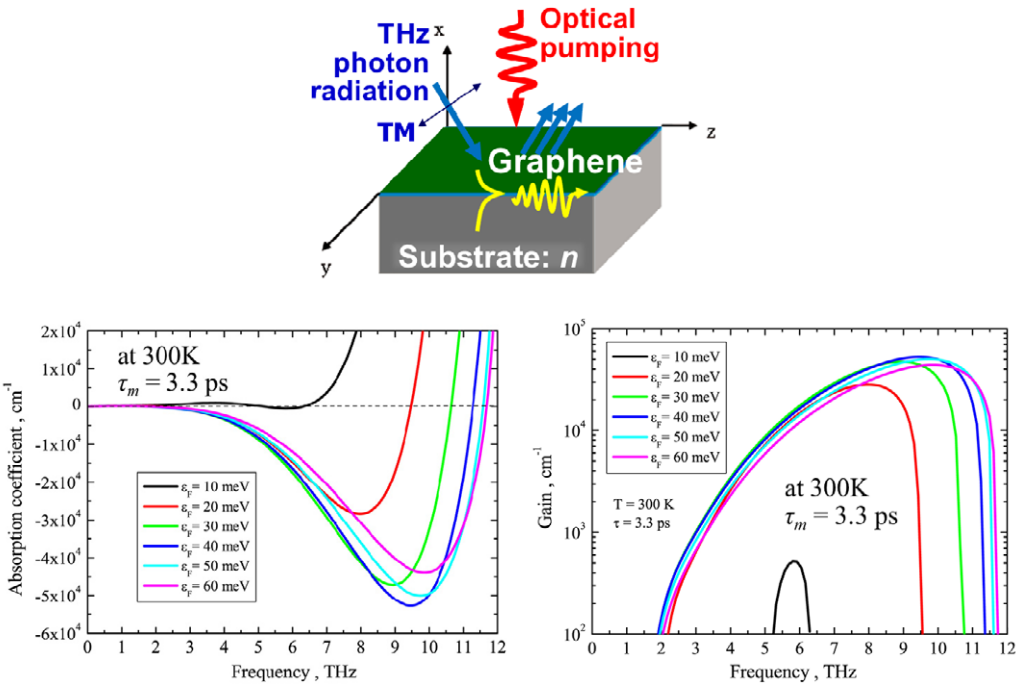

Figure 2. Frequency dependences of SPP absorption (left) and gain (right) for monolayer population-inverted graphene on SiO_2/Si substrate at 300 K for different quasi-Fermi energies $\varepsilon_F = 10$, 20, 30, 40, 50 and 60 meV. Carrier momentum relaxation time in graphene is $\tau_m = 3.3$ ps. The results demonstrate giant THz gain (negative values of absorption) of the order of 10^4 cm^{-1}.

in figure 3, which is identical to the one described in [19] and is based on a time-resolved near-field reflective electro-optic sampling with an fs-IR laser pulse for optical pumping and a synchronously generated THz pulse for probing the THz dynamics of the sample in a THz photon-echo manner. A 140 μm thick CdTe crystal acting as a THz probe pulse emitter as well as an electro-optic sensor was placed on an exfoliated monolayer-graphene/SiO_2/Si sample. A femtosecond-pulsed fiber laser with a full-width at half-maximum of 80 fs, repetition rate of 20 MHz and average power of ~4 mW was used as the optical pump and probe source. The laser is split into two paths used for pump and probe. The pumping laser beam, being linearly polarized, is mechanically chopped at ~1.2 kHz (for lock-in detection) and focused with a beam diameter of about 120 μm onto the sample and the CdTe from the back side, while the probing beam is cross polarized with respect to the pump beam and focused from the top side. The CdTe can rectify the optical pump pulse to emit the envelope THz probe pulse. The emitted primary THz beam grows along the Cherenkov angle to be detected at the CdTe top surface as the primary pulse (marked with '①' in figure 3(b)), and then reflects being subject to the graphene sample. When the substrate of the sample is conductive, the THz probe pulse transmitting through graphene again reflects back to the CdTe top surface, which is electro-optically detected as a THz photon echo signal (marked with '②' in figure 3(b)). Therefore, the original temporal response consists of the first forward propagating THz pulsation (no interaction with graphene) followed by a photon echo signal (probing the graphene). The delay between these two pulsations is given by the total roundtrip propagation time of the THz probe pulse through the CdTe. The system bandwidth is estimated to be around 6 THz, mainly limited

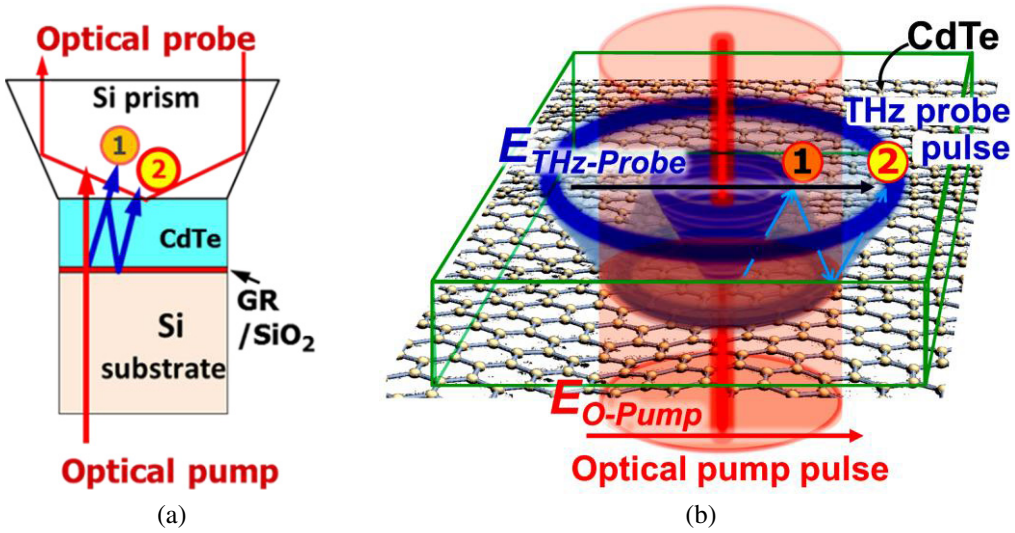

Figure 3. Experimental setup of the time-resolved optical pump, THz probe and optical probe measurement based on a near-field reflective electrooptic sampling. (a) Cross-sectional image of the pump/probe geometry, and (b) bird's-eye view showing the trajectories of the optical pump and THz probe beams. The polarization of the optical pump and the THz probe pulse are depicted with a red and a dark-blue arrow, respectively.

by the Reststrahlen band of the CdTe sensor crystal [19]. The roll off at higher frequency of the photon-echo spectrum starts at ∼2 THz, continuing monotonically till ∼4 THz and lasts at ∼6 THz [19].

The sample prepared for this experiment is a monolayer graphene, which was exfoliated from graphite and transferred onto a SiO_2/Si substrate, and is identical to the one used in [19, 20]. The graphene sample was characterized by the surface morphology using the atomic-force microscopy, the crystallographic properties using the Raman spectroscopy, the doping effects using the Hall-effect measurement and the microscopic surface potential distribution (fluctuation) using the Kelvin-force microscopy as shown in [19, 20]. The flake size of the graphene was ∼7000 μm^2. The momentum relaxation time was characterized to be 3.5 ps from the G-band to-D-band peak intensity ratio of the Raman spectra as also shown in [19, 20]. Table 1 summarizes these properties.

3.2. Temporal profile and Fourier spectrum of the population-inverted graphene to the THz pulse irradiation

Figure 4(a) shows temporal responses measured on the monolayer graphene with the CdTe crystal for different pumping pulse intensities up to the maximum intensity $I_\Omega = 3 \times 10^7\,W\,cm^{-2}$ (equivalently with pump fluence of $2.4\,\mu J\,cm^{-2}$, almost one order of magnitude below the level of Pauli blocking). It is worth rephrasing that each temporal profile is composed of two peaks from optical rectification in CdTe and the THz photon echo signal. The measured time delay between these two pulsations of 3.5 ps is in good agreement with the round-trip propagation time of the THz probe pulse through the CdTe crystals [19]. It is clearly

Table 1. Graphene sample properties.

Synthesis:	Exfoliation from HOPG
Substrate:	300 nm thick SiO_2/560 μm thick Si (100) (resistivity: 0.005 Ω cm)
Flake size:	$\sim > 7000\ \mu m^2$
Surface height variation as variance:	0.142 nm (in 20 μm × 20 μm area)
Surface potential variation as variance:	4.02 meV (in 10 μm × 20 μm area)
Raman G-band peak to D-band peak intensity ratio:	~35
Estimated carrier momentum relaxation time:	3.3 ps at 300 K
Dirac voltage:	~0 V

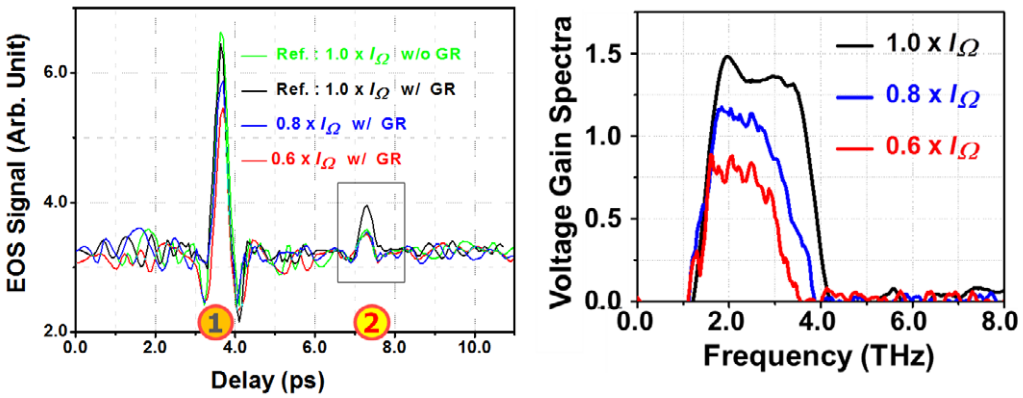

Figure 4. (a) Measured temporal responses of the THz photon-echo probe pulse (designated with '②') for different pumping intensities I_Ω (3×10^7 W cm^{-2}), $0.8 \times I_\Omega$ and $0.6 \times I_\Omega$. (b) Corresponding voltage gain spectra of graphene obtained by Fourier transforming the temporal responses of the secondary pulse measured at graphene flake, normalized to that at the position without graphene.

seen that the peak obtained on graphene is more intense than that obtained on the substrate without graphene, and that the obtained gain factor exceeds the theoretical limit given by the quantum conductance [21] by more than one order of magnitude, as was measured in [19]. We calculated the voltage gain spectra obtained by Fourier transforming the temporal responses of the secondary pulse, normalized to the frequency response without graphene as shown in figure 4(b). The measured waveforms and their corresponding gain spectra are well reproduced and showed similar pumping intensity dependence with the results shown in [19]. The roll off of the gain spectra at lower cutoff starts at ~2 THz and lasts at ~1.6 THz which is insensitive to the pumping intensity. On the other hand, the roll off at upper cutoff starts at ~3.5 THz at the maximum pumping intensity and lasts at ~4.1 THz, which seems to be limited by the measurement system bandwidth. The upper cutoff frequency decreases with decreasing the pumping intensity. Such a gain spectral dependence on pumping intensity qualitatively agrees with the theoretical calculations, but quantitatively exceeds by more than an order of the aforementioned quantum conductivity limit.

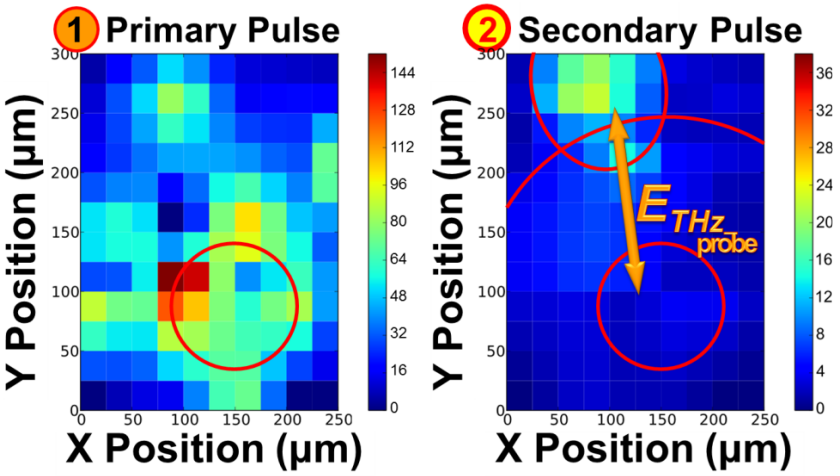

Figure 5. Spatial field distribution of the THz probe pulse intensities. The primary pulse shows nonpolar distribution, whereas the secondary pulse shows a strong localization to the area in which the THz probe pulse is impinged to the graphene surface in the TM modes.

3.3. Spatial field distribution of the THz probe pulse intensities

We observe the spatial distribution of the THz probe pulse under the linearly polarized optical pump and THz probe pulse conditions. To measure the in-plane spatial distributions of the THz probe pulse radiation, the optical probe pulse position (at the top surface of the CdTe crystal) was changed step-by-step by moving the incident point of the optical pump pulse. The pumping intensity I_Ω was fixed at the maximum level $3 \times 10^7\,\mathrm{W\,cm^{-2}}$. We measured ten times at every point with and without graphene, respectively, and took averages to obtain the electric field intensities and resultant Fourier transform spectra. Observed field distributions for the primary and secondary pulse intensities are shown in figure 5. The primary pulse field is situated along the circumference with diameter $\sim$50 μm concentric to the center of optical pumping position. On the other hand, the secondary pulse (THz photon echo) field is concentrated only at the restricted spot area on and out of the concentric circumference with diameter $\sim$150 μm, where the incoming THz probe pulse takes a TM mode capable of exciting the SPPs in graphene. The distance between the primary pulse position to the secondary pulse position is $\sim$100 μm or longer. The observed field distribution reproduces the reasonable trajectory of the THz echo pulse propagation in the TM modes inside the CdTe crystal as shown in figure 2 when we assume the Cherenkov angle of 30°, which was determined by the fraction of the refractive indices between infrared and THz frequencies.

How to couple the incoming/outgoing THz pulse photons to the surface plasmons in graphene is the point of discussion, because the defectless and flat surface of graphene itself has no structural feature that can excite the SPPs. One possibility of the excitation of SPPs by the incoming THz probe pulse is the spatial charge-density modulation at the area of photoexcitation by optical pumping. The pump beam having a Gaussian profile with diameter $\sim$120 μm may define the continuum SPP modes in a certain THz frequency range as seen in various SPPs waveguide structures [30, 31]. After a short propagation of the order of $\sim$10 μm, the SPPs approach the edge boundary of the illuminated and dark area so that they could mediate the

THz electromagnetic emission [32, 33]. The plasmon group velocity in graphene (exceeding the Fermi velocity) and propagation distance gives a propagation time of the order of 100 fs. According to the calculated gain spectra shown in figure 2(b), the gain enhancement factor could reach or exceed ∼10 at the gain peak frequency 4 THz, which is dominated in the optically probed secondary pulse signals. The obtained gain enhancement factor is $\gtrsim$50, which is still somewhat higher than the calculated results whose causes should be clarified in a further study.

4. Conclusion

Nonlinear carrier relaxation/recombination dynamics and the resultant stimulated THz photon emission with the excitation of SPPs in photoexcited monolayer graphene was experimentally studied using an optical-pump/THz-probe and optical probe measurement. The spatial distribution of the THz probe pulse intensities under linear polarization of the optical pump and THz probe pulses was measured. It was clearly observed that an intense THz probe pulse was detected only at the area where the incoming THz probe pulse takes a TM mode capable of exciting the SPPs. The observed gain factor is in fair agreement with theoretical calculations. Experimental results support the occurrence of the gain enhancement effect by the excitation of SPPs on THz stimulated emission in optically pumped monolayer graphene.

Acknowledgments

We thank V V Popov at Kotelnikov Institute of Radio Engineering and Electronics, Russia, M S Shur at Rensselaer Polytechnic Institute, USA, M Ryzhii at CNEL, University of Aizu and E Sano at RCIQE, Hokkaido University, Japan, for their contributions. This work was financially supported in part by JST-CREST, JSPS-GA-SPR (no. 23000008), JSPS Core-to-Core, Japan and NSF-PIRE-TeraNano, USA.

References

[1] Novoselov K S, Geim A K, Morozov S V, Jiang D, Zhang Y, Dubonos S V, Grigorieva I V and Frisov A A 2004 *Science* **306** 666
[2] Geim K and Novoselov K S 2007 *Nature Mater.* **6** 183
[3] Castro Neto A H, Guinea F, Peres N M R, Novoselov K S and Geim A K 2009 *Rev. Mod. Phys.* **81** 109–62
[4] Bonaccorso F, Sun Z, Hasan T and Ferrari A C 2010 *Nature Photon.* **4** 611–22
[5] Grigorenko A N, Polini M and Novoselov K S 2012 *Nature Photon.* **6** 749–58
[6] Ryzhii V, Ryzhii M and Otsuji T 2007 *J. Appl. Phys.* **101** 083114
[7] Ryzhii M and Ryzhii V 2007 *Japan. J. Appl. Phys.* **46** L151
[8] Ryzhii V, Ryzhii M, Mitin V and Otsuji T 2011 *J. Appl. Phys.* **110** 094503
[9] Satou A, Otsuji T and Ryzhii V 2011 *Japan. J. Appl. Phys.* **50** 070116
[10] Ryzhii V, Ryzhii M, Mitin V, Satou A and Otsuji T 2011 *Japan. J. Appl. Phys.* **50** 094001
[11] Satou A, Ryzhii V, Kurita Y and Otsuji T 2013 *J. Appl. Phys.* **113** 143108
[12] Dubinov A A, Aleshkin V Y, Ryzhii M, Otsuji T and Ryzhii V 2009 *Appl. Phys. Express* **2** 092301
[13] Ryzhii V, Ryzhii M, Satou A, Otsuji T, Dubinov A A and Aleshkin V Y 2009 *J. Appl. Phys.* **106** 084507
[14] Ryzhii V, Dubinov A, Otsuji T, Mitin V and Shur M S 2010 *J. Appl. Phys.* **107** 054505
[15] Dawlaty J M, Shivaraman S, Chandrashekhar M, Rana F and Spencer M G 2008 *Appl. Phys. Lett.* **92** 042116
[16] George P A, Strait J, Dawlaty J, Shivaraman S, Chandrashekhar M and Spencer F R M G 2008 *Nano Lett.* **8** 4248

[17] Breusing M, Ropers C and Elsaesser T 2009 *Phys. Rev. Lett.* **102** 086809
[18] Li T, Luo L, Hupalo M, Zhang J, Tringides M C, Schmalian J and Wang J 2012 *Phys. Rev. Lett.* **108** 167401
[19] Boubanga-Tombet S, Chan S, Watanabe T, Satou A, Ryzhii V and Otsuji T 2012 *Phys. Rev.* B **85** 035443
[20] Otsuji T, Boubanga Tombet S A, Satou A, Fukidome H, Suemitsu M, Sano E, Popov P, Ryzhii M and Ryzhii V 2012 *J. Phys. D: Appl. Phys.* **45** 303001
[21] Falkovsky L and Varlamov A 2007 *Eur. Phys. J.* B **56** 281
[22] Dubinov A A, Aleshkin Y V, Mitin V, Otsuji T and Ryzhii V 2011 *J. Phys.: Condens. Matter* **23** 145302
[23] Ryzhii V, Satou A and Otsuji T 2007 *J. Appl. Phys.* **101** 024509
[24] Rana F 2008 *IEEE Trans. Nanotechnol.* **7** 91–9
[25] Wright A R, Cao J C and Zhang C 2009 *Phys. Rev. Lett.* **103** 207401
[26] Strait J H, Wang H, Shivaraman S, Shields V, Spencer M and Rana F 2011 *Nano Lett.* **11** 4902–6
[27] Winzer T, Knorr A and Malic E 2010 *Nano Lett.* **10** 4839–43
[28] Winzer T and Malic E 2012 *Phys. Rev.* B **85** 241404
[29] Nair R R, Blake P, Grigorenko A N, Novoselov K S, Booth T J, Stauber T, Peres N M R and Geim A K 2008 *Science* **320** 1308
[30] He X Y, Wang Q J and Yu S F 2012 *Plasmonics* **7** 571–7
[31] He X Y 2009 *Opt. Express* **17** 15359–71
[32] Lawrie B J, Haglund R F Jr and Mu R 2009 *Opt. Express* **17** 2565
[33] Wedge S and Barnes W 2004 *Opt. Express* **12** 3672